FULL PAPER

The Effective Electron-Transfer Distance in Dinuclear Ruthenium Complexes Containing the Unsymmetrical Bridging Ligand 3,5-Bis(2-pyridyl)-1,2,4-triazolate

Deanna M. D'Alessandro,[a] Peter H. Dinolfo,[b] Joseph T. Hupp,[b] Peter C. Junk,[c][‡] and F. Richard Keene*[a]

Electroabsorption (Stark effect) measurements on the inter-valence charge-transfer (IVCT) transitions in the diastereo-isomers of $[\{Ru(bpy)_2\}_2(\mu\text{-bpt}^-)]^{4+}$ [bpy = 2,2′-bipyridine, bpt⁻ = 3,5-bis(2-pyridyl)-1,2,4-triazolate] in *n*-butyronitrile glass at 77 K reveal effective charge-transfer distances of 5.92 ± 0.03 Å for the $\Delta\Lambda/\Lambda\Delta$ form and 5.44 ± 0.04 Å for the $\Delta\Delta/\Lambda\Lambda$ form. These values correspond to approximately 95 and 88 %, respectively, of the geometrical metal–metal distance

of 6.185(10) Å, obtained from the X-ray crystal structure of the cation in the related complex $(\Delta\Lambda)\text{-}[\{Ru(Me_2bpy)_2\}_2(\mu\text{-bpt}^-)](PF_6)_3$. The results are consistent with a localized Class II classification for the mixed-valence systems $[\{Ru(pp)_2\}_2(\mu\text{-bpt}^-)]^{4+}$, where pp = bpy, Me₂bpy = 4,4′-dimethyl-2,2′-bipyridine.
(© Wiley-VCH Verlag GmbH & Co. KGaA, 69451 Weinheim, Germany, 2006)

Introduction

Dinuclear polypyridyl complexes of ruthenium and osmium based on di-bidentate polypyridyl bridging ligands have been the subject of extensive research efforts over the past two decades, as part of rapid advances in metallosupramolecular chemistry. Bridging ligands provide the linkage between the metal centers in polymetallic assemblies and control the distances and relative orientations of the components, as well as the inter-component electron- and energy-transfer processes.[1–8]

The anion of 3,5-bis(2-pyridyl)-1,2,4-triazole (shown in Figure 1) is a particularly interesting bridging ligand, as it carries a negative charge and exhibits a high σ-donor and low π-acceptor ability.[9] As a consequence, bpt⁻ constitutes a member of a relatively small class of bridging ligands, which mediate the electronic coupling between the metal centers (denoted by M¹ and M² in Figure 1) by a hole-transfer mechanism. Because these ligands possess electron-

rich high-lying π* orbitals, the decisive factor in the metal–metal coupling is the energy gap between the highest-occupied molecular orbitals (HOMOs) of the bridge and the metal-based dπ orbitals, as shown in Figure 2.[6]
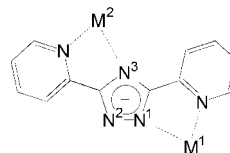

Figure 1. The 3,5-bis(2-pyridyl)-1,2,4-triazolate (bpt⁻) bridging ligand. M¹ and M² denote the metal centers coordinated at the N¹ and N³ sites, respectively.

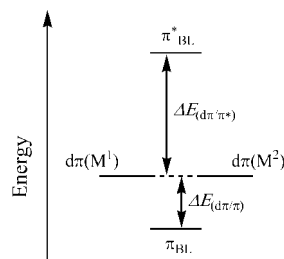
Figure 2. Schematic energy level diagrams for superexchange-assisted electronic coupling by a *hole-transfer* mechanism.[6] M¹ and M² denote the metal centers and BL denotes the bridging ligand.

The coupling between M¹ and M² can involve direct contributions from a "through-space" mechanism, and/or indirect contributions from a "through-bond" superexchange process where the bridging ligand mediates the donor-ac-

[a] School of Pharmacy and Molecular Sciences, James Cook University,
Townsville, Queensland 4811, Australia
Fax: +61-7-4781-6078
E-mail: Richard.Keene@jcu.edu.au
[b] Department of Chemistry, Northwestern University,
211 Sheridan Road, Evanston, IL 60208-3113, USA
[c] School of Pharmacy and Molecular Sciences, James Cook University,
Townsville, Queensland 4811, Australia
[‡] Present address: Department of Chemistry, Monash University,
Clayton, Victoria 3800, Australia
☐ Supporting information for this article is available on the WWW under http://www.eurjic.org or from the author.

ceptor coupling. In the latter case, the superexchange theory[10] provides a conceptual framework for bridging ligand effects in intramolecular electron transfer.[5,6] The parameters, which are effective to describe the through-bond interaction are the overlap between the frontier orbitals of the metals, $d\pi(M^1)$ and $d\pi(M^2)$, and the bridging ligand (π_{BL} and $\pi_{BL}*$), and the electronic interactions between the atoms of the bridge connecting the frontier units to one another.

In dinuclear complexes incorporating bpt⁻, the coordination environments of the two metal centers are chemically distinct due to the enhanced σ-donor ability of the N^1 ($\equiv N^2$) position of the triazolate ring relative to the N^3 position.[11] As a consequence, a "redox asymmetry" (denoted by ΔE_0) exists between the inequivalent coordination sites.[12,13]

The classical theory developed by Hush[14,15] provides a conceptual framework for the contribution of redox asymmetry effects to the electron-transfer barrier through the analysis of the intervalence charge-transfer (IVCT) transitions generated in the mixed-valence forms of dinuclear complexes. In accordance with Equation (1), the energy (ν_{max}) of an IVCT band, which is typically observed in the near-infrared (NIR) region of the absorption spectrum of the mixed-valence complex, is given in terms of the redox asymmetry and the Franck-Condon reorganizational energy contributions. The latter are composed of an inner-sphere component (λ_i) due to bond length and angle rearrangement, and also an outer-sphere component (λ_o) due to solvent and anion rearrangement in the secondary coordination sphere.[14,15]

$$\nu_{max} = = \lambda_i + \lambda_o + \Delta E_0 \qquad (1)$$

In recent work from our laboratory, comparisons between the characteristics of the IVCT transitions, generated by the mixed-valence forms of the diastereoisomers, ($\Delta\Lambda/\Lambda\Delta$)- and ($\Delta\Delta/\Lambda\Lambda$)-[{Ru(bpy)$_2$}$_2$(μ-BL)]$^{n+}$ (BL = a range of bis-bidentate polypyridyl bridging ligands) have revealed a stereochemical dependence of the IVCT energies, intensities and bandwidths. The origins of such dependencies have been ascribed to redox asymmetry contributions to Equation 1) due to stereochemically-directed structural distortions[16] and ion-pairing interactions,[17] as well as the outer-sphere reorganizational contributions due to spatially-directed solvent interactions.[18] The present work broadens our investigation into the use of stereoisomers as probes for the factors that govern the electron-transfer barrier through the characterization of the IVCT transitions in the $\Delta\Lambda/\Lambda\Delta$ and $\Delta\Delta/\Lambda\Lambda$ diastereoisomers of [{Ru(pp)$_2$}$_2$(μ-bpt⁻)]$^{4+}$ (pp = bpy, Me$_2$bpy), shown in Figure 3. Electroabsorption (Stark effect) measurements on the IVCT bands of the diastereoisomers of [{Ru(bpy)$_2$}$_2$(μ-bpt⁻)]$^{4+}$ provide a measure of the *effective* charge-transfer distances, which may be shortened relative to the geometric metal–metal distances due to electronic delocalization, self-polarization and other effects.[19–23] Whereas Browne and co-workers[24] concluded that the stereoisomeric identity of the $\Delta\Lambda$, $\Lambda\Delta$, $\Delta\Delta$ and $\Lambda\Lambda$ forms of [{Ru(bpy)$_2$}$_2$(μ-bpt⁻)]$^{3+}$ had no influence on the

photophysical properties of the complexes either at 77 K or room temperature, the influence of stereochemical effects on the IVCT properties of the systems were not addressed. Previous studies have, however, reported the redox and spectroscopic characteristics,[9,11,12,25–27] resonance Raman spectra[28] and photophysical behavior[9,29] of stereoisomeric mixtures of the homo- and hetero-dinuclear complexes of ruthenium, osmium, rhodium and iridium incorporating bpt⁻ and its protonated analog, Hbpt.
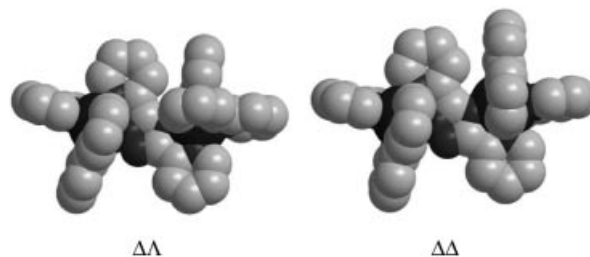

Figure 3. Schematic representations of ($\Lambda\Lambda$)- and ($\Delta\Delta$)-[{Ru(bpy)$_2$}$_2$-(μ-bpt⁻)]$^{3+}$; hydrogen atoms are omitted for clarity.

It must be noted that due to the inequivalence of the metal coordination sites, the $\Delta\Lambda/\Lambda\Delta$ form comprises a pair of geometric isomers. No attempt was made to separate the geometric forms in the present report.

The understanding of the fundamental stereochemical effects on the IVCT transitions in dinuclear complexes has important implications for the elucidation of spatial influences on electron migration in natural processes such as photosynthesis. Because the unsymmetrical component in bpt⁻ may be exploited to facilitate vectorial electron- and energy-transfer processes in polynuclear complexes, which form the basis of novel molecular-scale devices,[9,11,12,24,25,27–40] stereochemical effects may also offer a novel means of "fine-tuning" the metal–metal interactions.

Results and Discussion

Diastereoisomer Synthesis, Separation and Structural Characterization: The complex [{Ru(bpy)$_2$}$_2$(μ-bpt⁻)]$^{3+}$ has been synthesized previously by the reaction of [Ru(bpy)$_2$-Cl$_2$]·2H$_2$O with bpt in ethanol/water (2:1) under reflux.[11,33] In the present case, an alternative microwave-assisted methodology was employed[16,41–44] which produced equivalent or increased reaction yields of the dinuclear species compared with the thermal method; however, there was a significant reduction in the reaction times.

The chromatographic separation of the diastereoisomers of [{Ru(bpy)$_2$}$_2$(μ-bpt⁻)]$^{3+}$ by a semi-preparative HPLC technique has been reported previously;[24] in the present report, the separation was achieved using a cation-exchange chromatographic procedure with SP Sephadex C-25 as the support and aqueous solutions of sodium toluene-4-sulfonate as the eluent. The band 1 and 2 eluates were determined to be the $\Delta\Lambda/\Lambda\Delta$ and $\Delta\Delta/\Lambda\Lambda$ diastereoisomers, respectively. Interestingly, the two forms exhibited different colors on the column, with the $\Delta\Lambda/\Lambda\Delta$ form displaying a

red, and the $\Delta\Delta/\Lambda\Lambda$ form displaying an orange coloration. During the procedure, a small amount of smearing was observed as the complex passed down the column. This was attributed to the presence of an uncoordinated nitrogen atom on the triazole ring of the bpt⁻ bridging ligand. Measurements on the pH dependence of the absorption spectrum of [{Ru(bpy)$_2$}$_2$(μ-bpt⁻)]$^{3+}$ by Hage et al.[11] revealed a pK_a of -0.6 ± 0.3 for the complex in aqueous solution. This suggests that the protonation of the free nitrogen atom under the conditions employed in the chromatographic separation is unlikely.

Because poor microanalysis figures were obtained, the characterization and purity assessment of the diastereoisomers were based on the NMR spectra and electrochemical data. Incomplete combustion may in part account for these unsatisfactory figures;[45] however, the occlusion of variable numbers of solvent molecules and counter-anions may also be a factor. Such difficulties have previously been noted for dinuclear complexes of ruthenium(II).[46]

The ¹H numbering schemes for the ligands in [{Ru(bpy)$_2$}$_2$(μ-bpt⁻)]$^{4+}$ are shown in Figure S1 (Supporting Information; see footnote on the first page of this article) and the assignments of the spectra were performed with the assistance of ¹H COSY spectra.[47] The coordinated bpy ligands exhibited the expected coupling constant values[48] ($J_{3,4} = 8$, $J_{3,5} = 1.5$, $J_{4,5} = 8$, $J_{4,6} = 1.5$ Hz and $J_{5,6} = 5$ Hz) and coupling patterns based on the symmetry requirements of the complexes.

The assignment of the ¹H resonances associated with individual terminal ligands was based on the differential anisotropic effects of the two ligands above (and below) the plane of the bridging ligand. Because an analysis of the ¹H NMR spectra of the diastereoisomers of [{Ru(bpy)$_2$}$_2$(μ-bpt⁻)]$^{3+}$ have been reported previously,[11] the assignments for the diastereoisomers of [{Ru(pp)$_2$}$_2$(μ-bpt⁻)]$^{3+}$ in the present investigation are listed in the Experimental Section only.

Structural Considerations: X-Ray Crystallography

A limited number of crystal structures have been reported of dinuclear ruthenium complexes incorporating polypyridyl ligands. Of the three examples of dinuclear species containing unsymmetrical bridging ligands,[12,49] two have contained the bpt⁻ bridging ligand. In both cases, the crystals were obtained in the $\Delta\Lambda/\Lambda\Delta$ form during an attempt to separate the diastereoisomers of the complexes through fractional crystallization. Accordingly, the single crystals of $(\Delta\Lambda/\Lambda\Delta)$-[{Ru(Me$_2$bpy)$_2$}$_2$(μ-bpt⁻)](PF$_6$)$_3$ obtained in the present investigation represent the first example of the selective isolation of one of the components containing an unsymmetrical bridging ligand *prior* to crystal growth.

Figure 4 shows the X-ray crystal structure for the cation in $(\Delta\Lambda/\Lambda\Delta)$-[{Ru(Me$_2$bpy)$_2$}$_2$(μ-bpt⁻)](PF$_6$)$_3$. The complex crystallises in the triclinic space group $P\bar{1}$ with two dinuclear cations in the unit cell. A summary of the crystal data

and refinement are provided in Table S1 (Supporting Information). The ruthenium–nitrogen distances of 2.026(10)–2.109(10) Å correlate with those published for previous structures.[12,50–52] The Ru(2)–N(1) distance of 2.004(9) Å is significantly shorter than the Ru(1)–N(3) distance of 2.109(10) Å, which is consistent with the enhanced σ-donor ability of the N(1) site of the triazolate ring compared with the N(3) site.[9,11,12,27,33] The bond lengths and angles of the terminal Me$_2$bpy ligands are in the normal range for complexes incorporating [Ru(Me$_2$bpy)$_2$]$^{2+}$ and [Ru(bpy)$_2$]$^{2+}$ moieties.[12,50–52] The "bite-angles" of the terminal chelating ligands vary between 78.1(5)° and 79.4(5)°, which is typical for bipyridine-like ligands.[12,50–52]
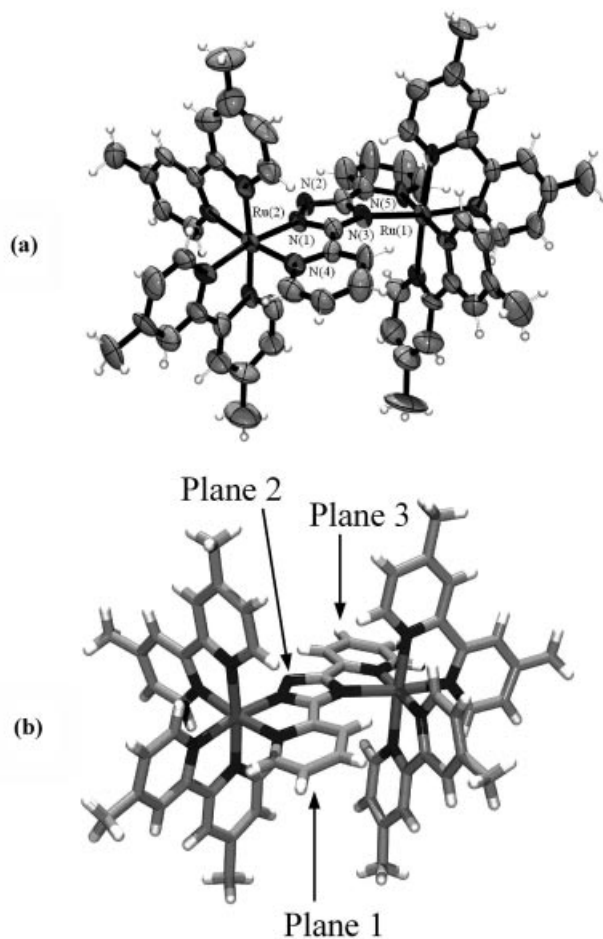

Figure 4. (a) Partial atom labelling, and (b) designation of the planes for the cation in $(\Delta\Lambda/\Lambda\Delta)$-[{Ru(Me$_2$bpy)$_2$}$_2$(μ-bpt⁻)](PF$_6$)$_3$.

As shown in Figure 4 (b), the dihedral angles between the least-squares plane of the triazolate ring (plane 2) and the planes of the two pyridine rings (planes 1 and 3) are 10.8(5)° and 8.63(5)°, respectively, indicating a considerable deviation from planarity of the bpt⁻ ligand after the coordination of two [Ru(Me$_2$bpy)$_2$]$^{2+}$ moieties. This distortion appears to arise from steric crowding between the methyl groups oriented perpendicular to the "long axis" of the bridge. The methyl groups located "above" the plane of the bridging ligand induce a curvature in the bridge, which re-

sults in the pyridyl groups bending downwards away from the normal bridging plane. In the representation of the $\Delta\Delta/\Lambda\Lambda$ diastereoisomer shown in Figure 3, one might anticipate less structural distortion relative to the $\Delta\Lambda/\Lambda\Delta$ form, as the potentially unfavorable interactions between the methyl groups are avoided due to the parallel orientation of the terminal ligands above (and below) the bridging plane. The Ru(1)···Ru(2) separation is 6.185(10) Å.

Electrochemical and UV/Vis/NIR Spectral Characterization

The redox potentials for the E_{ox1} ([5+/4+]; i.e. Ru^{III}–Ru^{II}/Ru^{II}–Ru^{II}) and E_{ox2} ([6+/5+]; i.e. Ru^{III}–Ru^{III}/Ru^{III}–Ru^{II}) couples for ($\Delta\Lambda/\Lambda\Delta$)- and ($\Delta\Delta/\Lambda\Lambda$)-[{Ru(pp)$_2$}$_2$($\mu$-bpt$^-$)]$^{4+}$ (pp = bpy, Me$_2$bpy) were investigated by cyclic and differential pulse voltammetry in acetonitrile containing 0.1 M [(n-C$_4$H$_9$)$_4$N]PF$_6$, and are reported in Table 1. ΔE_{ox} defines the potential difference between the [6+/5+] and [5+/4+] couples. The full electrochemical characteristics of the diastereoisomers [{Ru(bpy)$_2$}$_2$(μ-bpt$^-$)]$^{4+}$ in 0.1 M [(n-C$_4$H$_9$)$_4$N]-

Table 1. Electrochemical data (in mV relative to the Fc$^+$/Fc^0 couple) and comproportionation constants (K_c) for [{Ru(pp)$_2$}$_2$(μ-bpt$^-$)]$^{3+}$ in 0.1 M [(n-C$_4$H$_9$)$_4$N]PF$_6$/CH$_3$CN.

Complex	$K_c^{[a]}$ ($\times 10^{-5}$)	$\Delta E_{ox}^{[b]}$	E_{ox2}	E_{ox1}
($\Delta\Lambda/\Lambda\Delta$)-[{Ru(bpy)$_2$}$_2$($\mu$-bpt$^-$)]$^{3+}$	1.88	312	992	680
($\Delta\Delta/\Lambda\Lambda$)-[{Ru(bpy)$_2$}$_2$($\mu$-bpt$^-$)]$^{3+}$	1.61	308	992	684
($\Delta\Lambda/\Lambda\Delta$)-[{Ru(Me$_2$bpy)$_2$}$_2$($\mu$-bpt$^-$)]$^{3+}$	5.58	340	927	587
($\Delta\Delta/\Lambda\Lambda$)-[{Ru(Me$_2$bpy)$_2$}$_2$($\mu$-bpt$^-$)]$^{3+}$	3.78	330	902	572

[a] K_c values are given by $K_c = \exp(\Delta E_{ox}F/RT)$ where $F/RT = 38.92$ V^{-1} at 298 K. [b] $\Delta E_{ox} = E_{ox2} - E_{ox1}$. Potentials are quoted ±3 mV.

PF$_6$ and 0.02 M [(n-C$_4$H$_9$)$_4$N]{B(C$_6$F$_5$)$_4$} electrolytes have been reported previously.[53]

The dinuclear systems are each characterized by two reversible one-electron redox processes corresponding to successive oxidation of the metal centers, in addition to multiple reversible ligand-based reductions in the cathodic region. The effect of terminal ligand variation on the redox couples is consistent with the trends observed for the mononuclear complexes [Ru(pp)$_3$]$^{2+}$ (pp = bpy, Me$_2$bpy);[54] the stronger σ-donor ability of Me$_2$bpy relative to bpy results in a less anodic potential for the first oxidation in the diastereoisomers of [{Ru(Me$_2$bpy)$_2$}$_2$(μ-bpt$^-$)]$^{3+}$.

The separation between the two metal-centered oxidations is larger for the diastereoisomers incorporating the Me$_2$bpy terminal ligands relative to those incorporating bpy ligands, and small differences are observed between the diastereoisomeric forms of the same complex. As an increase in delocalization leads to a decrease in the magnitude of ΔE_{ox} for electron-rich bridging ligands such as bpt$^-$,[2] the results suggest that delocalization is enhanced for the bpy-based diastereoisomers. It should be noted, however, that these differences cannot be solely ascribed to variations in the extent of electronic delocalization, as the magnitude of ΔE_{ox} also reflects contributions from ion-pairing interactions,[53] solvation energies and statistical factors.[4,55]

Electronic Spectroscopy and Spectroelectrochemistry

The UV/Vis/NIR spectroscopic data for the un-oxidized (+3), mixed-valence (+4) and fully-oxidized (+5) forms of ($\Delta\Lambda/\Lambda\Delta$)- and ($\Delta\Delta/\Lambda\Lambda$)-[{Ru(pp)$_2$}$_2$($\mu$-bpt$^-$)]$^{n+}$ for the range 3050-30000 cm^{-1} are characterized by a combination of overlapping dπ(Ru^{II}) → π*(pp, bpt$^-$) singlet metal-to-ligand (^{1}MLCT) transitions. The lowest energy-absorption band is assigned as a dπ(Ru^{II}) → π*(pp) transition.
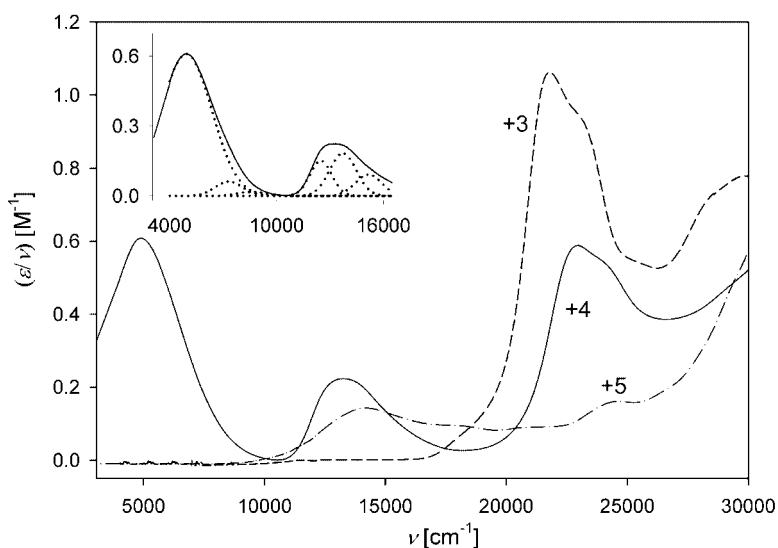

Figure 5. UV/Vis/NIR spectra of the reduced absorption spectra, (ε/ν) vs. ν, of ($\Delta\Lambda/\Lambda\Delta$)-[{Ru(bpy)$_2$}$_2$($\mu$-bpt$^-$)]$^{n+}$; n = 3 (------), 4 (——), 5 (–·–·–) in 0.1 M [(n-C$_4$H$_9$)$_4$N]PF$_6$/CH$_3$CN at –35 °C. The inset shows the bands obtained by Gaussian deconvolution of the NIR spectra (······).

Table 2. UV/Vis/NIR spectroscopic data of the reduced absorption spectra (ε/ν vs. ν) for the mono- and dinuclear complexes in 0.1 M [(n-$C_4H_9)_4N]PF_6/CH_3CN$ at –35 °C.[a] The NIR spectroscopic data are indicated in bold type.[a]

Complex	n	ν_{max} [cm^{-1}] $\{(\varepsilon/\nu)_{max}$ [M^{-1}]$\}$[a]	
		bpy	Me2bpy
($\Delta\Lambda/\Lambda\Delta$)-[{Ru(pp)$_2$}$_2$($\mu$-bpt$^-$)]$^{n+}$	3	21810 (1.063)	21720 (1.015)
		sh 23090 (0.9332)	sh 22880 (0.9136)
	4	**4930 (0.6094)**	**4730 (0.5517)**
		13210 (0.2340)	13720 (0.1890)
		22930 (0.6034)	22820 (0.6364)
		sh 24000 (0.5620)	sh 23750 (0.6048)
	5	14190 (0.1428)	14710 (0.1218)
		24650 (0.1634)	22610 (0.2124)
($\Delta\Delta/\Lambda\Lambda$)-[{Ru(pp)$_2$}$_2$($\mu$-bpt$^-$)]$^{n+}$	3	21880 (1.044)	21780 (1.031)
		sh 23930 (0.9332)	sh 22980 (0.9220)
		29200 (0.7611)	29410 (0.7204)
	4	**5030 (0.5043)**	**4920 (0.5542)**
		13450 (0.2170)	13790 (0.1848)
		22920 (0.5750)	22780 (0.6232)
	5	14340 (0.1563)	14890 (0.1302)
		22710 (0.2218)	22710 (0.2320)
[Ru(bpy)$_2$(bpt$^-$)]$^{n+}$	1	21830 (0.5022)	
		23240 (0.4758)	
		sh 25720 (0.3517)	
	2	12930 (0.1449)	
		21490 (0.1408)	

[a] ν_{max} ±10/cm^{-1} and $(\varepsilon/\nu)_{max}$ ±0.001/M^{-1}; sh = shoulder band.

The UV/Vis/NIR spectra for ($\Delta\Lambda/\Lambda\Delta$)-[{Ru(pp)$_2$}$_2$($\mu$-bpt$^-$)]$^{n+}$ (n = 3, 4, 5) at –35 °C are shown in Figure 5, and the full details of the spectroscopic data for the series of complexes are reported in Table 2. Spectroelectrochemical generation of the +4 and +5 forms of the diastereoisomers revealed stable isosbestic points in the spectral progressions accompanying both oxidation processes. The ^{1}MLCT absorption bands decreased in intensity on one-electron oxidation and collapsed on further oxidation to the +5 species. The formation of the mixed-valence complex was also characterized by the appearance of two new bands in the regions 5000–5500 cm^{-1} and 13000–14500 cm^{-1}. The former was assigned as an IVCT band and disappeared on further oxidation to the +5 state. The band at 13000–14500 cm^{-1} experienced a slight blue-shift on oxidation to the +5 state, and was assigned as a π(bpy) → dπ(Ru^{III}) ligand-to-metal charge-transfer (LMCT) transition, consistent with the LMCT transition at 12930 cm^{-1} in [Ru(bpy)$_2$(bpt$^-$)]$^{2+}$ (see Table 2 and Figure S2 in the Supporting Information). As shown in the inset in Figure 5, the LMCT transition is composed of three underlying Gaussian-shaped transitions, which may arise due to the non-equivalence of the Ru centers bound to the N^1 and N^3 coordination sites in bpt$^-$ (Figure 1).

Intervalence Charge Transfer

An overlay of the NIR spectra of the diastereoisomers of the mixed-valence systems [{Ru(pp)$_2$}$_2$(μ-bpt$^-$)]$^{4+}$ is shown in Figure 6, and the results of the IVCT band maxima ν_{max}, molar absorption coefficients $(\varepsilon/\nu)_{max}$ and bandwidths $\Delta\nu_{1/2}$ derived from the deconvolution procedure are summarized in Table 3.
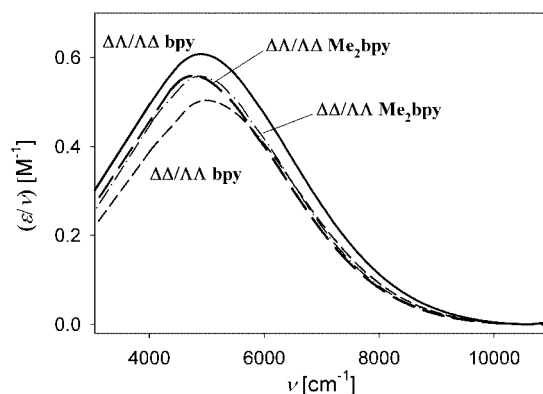

Figure 6. Overlay of the IVCT bands for the diastereoisomers of [{Ru(bpy)$_2$}$_2$(μ-bpt$^-$)]$^{4+}$ ($\Delta\Lambda/\Lambda\Delta$ and $\Delta\Delta/\Lambda\Lambda$) and [{Ru(Me$_2$bpy)$_2$}$_2$-($\mu$-bpt$^-$)]$^{4+}$ ($\Delta\Lambda/\Lambda\Delta$ and $\Delta\Delta/\Lambda\Lambda$) in 0.1 M [(n-$C_4H_9)_4N]PF_6/CH_3CN$ at –35 °C.

Whereas the IVCT properties for [{Ru(bpy)$_2$}$_2$(μ-bpt$^-$)]$^{4+}$ (as a diastereoisomeric mixture) have been discussed previously,[11,12,38,56] the influence of the inherent stereochemical identity of the systems on their intramolecular electron-transfer properties had not been addressed. In the present investigation, the diastereoisomers of [{Ru(pp)$_2$}$_2$(μ-BL)]$^{4+}$ (pp = bpy, Me$_2$bpy) are seen to exhibit Gaussian-shaped IVCT bands. Because the lower energy side of the bands was obscured by the detector limit, the electronic coupling parameters (H_{ab}) were determined from Equation (2).[57,58] For simplicity (and due to a lack of detailed information) the issue of multiple overlapping intervalence bands was ignored in estimating H_{ab}. The zeroth-order moments (M_0) of the IVCT bands [see Equation (i) below and Exp. Sect.] were obtained by doubling the band area on the high-en-

Table 3. Characteristics of the IVCT bands for the dinuclear mixed-valence complexes in 0.1 M [(n-C₄H₉)₄N]PF₆/CH₃CN at –35 °C. Parameters for overall envelope are shown in bold type: details of deconvoluted bands are in normal type.[a]

Complex	v_{max} [cm⁻¹]	$(\varepsilon/v)_{max}$ [M⁻¹]	$\Delta v_{1/2}$ [cm⁻¹]	$\Delta v_{1/2}°$ [cm⁻¹]	M_0 [M⁻¹]	$\|\mu_{12}\|$ [e·Å]	H_{ab} [cm⁻¹]
(ΔΛ/ΛΔ)-[{Ru(bpy)₂}₂(μ-bpt⁻)]⁴⁺	**4930**	**0.6094**	**3780**	2754	2473	1.024	817
	4930	0.6094	3770		2350		
	7315	0.0623	1808		120		
	8617	0.0177	1920		36.2		
	12486	0.1508	1450		233		
	13728	0.1835	1760		344		
	15164	0.0912	1770		165		
	16528	0.0376	1500		29.1		
(ΔΔ/ΛΛ)-[{Ru(bpy)₂}₂(μ-bpt⁻)]⁴⁺	**5030**	**0.5043**	**3660**	2786	1985	0.9178	746
	5030	0.0504	3450		1870		
	7630	0.0437	2266		105		
	12658	0.1523	1617		262		
	14010	0.1584	1710		288		
	15434	0.0808	1566		127		
	16490	0.0354	1104		21.2		
(ΔΛ/ΛΔ)-[{Ru(Me₂bpy)₂}₂(μ-bpt⁻)]⁴⁺	**4730**	**0.5517**	**3776**	2686	2275	0.9826	750
	4730	0.5517	3640		2010		
	6517	0.0672	1772		127		
	7550	0.0601	2345		149.9		
	12945	0.1381	1582		232		
	14269	0.1477	1678		264		
	15590	0.0649	1468		101		
	16688	0.0271	1492		43.0		
(ΔΔ/ΛΛ)-[{Ru(Me₂bpy)₂}₂(μ-bpt⁻)]⁴⁺	**4920**	**0.5542**	**3553**	2750	2140	0.9530	758
	4920	0.5542	3320		1970		
	6883	0.0276	1320		38.8		
	7935	0.0378	2080		83.6		
	12957	0.1399	1633		243		
	14260	0.1393	1670		248		
	15690	0.0834	1802		160		
	17070	0.0270	1405		40.3		

[a] The errors in the observed parameters are ±10 cm⁻¹ for v_{max}, M¹ and $\Delta v_{1/2}$, ±0.001 M⁻¹ for $(\varepsilon/v)_{max}$, ±5 M⁻¹ for M_0 and ±0.001 e·Å for $|\mu_{12}|$.

ergy half of the bands, and the transition moments, $|\mu_{12}|$, were subsequently determined from Equation (ii) (see Exp. Sect.). For all complexes, r_{ab} was initially equated with the through-space geometrical distance between the metal centers,[59] which was estimated as 6.185(10) Å from the X-ray crystal structure of (ΔΛ/ΛΔ)-[{Ru(Me₂bpy)₂}₂(μ-bpt⁻)]³⁺.

$$H_{ab} = \frac{|\mu_{12}|}{er_{ab}} v_{max} \qquad (2)$$

The IVCT manifolds were fitted by a Gaussian-shaped band, which reproduced the maximum energy and intensity, as shown by the deconvolution for (ΔΛ/ΛΔ)-[{Ru(bpy)₂}₂-(μ-bpt⁻)]⁴⁺ in the inset in Figure 5. Additional minor Gaussian-shaped bands were required to reproduce the bandwidth on the high-energy side. From a classical two-state analysis[60] of the IVCT transitions, the predicted bandwidth is given by Equation (3), where $16RT\ln2 = 1836$ cm⁻¹ at 238 K. ΔE_0 represents the energy difference induced by the unsymmetrical coordination environment, and has been estimated as 800 cm⁻¹ from electrochemical measurements on the two isomers of [Ru(bpy)₂(pyridyltri-azole)]²⁺.[12,13]

$$\Delta v_{1/2}° = [16RT\ln2(\lambda - \Delta E_0)]^{1/2} \qquad (3)$$

On the basis of the broad bandwidths compared with the theoretical bandwidths in Table 3, the complexes may be classified as localized Class II systems within the Robin and Day classification scheme.[61]

As electronic coupling decreases the *effective* electron-transfer distance relative to the geometrical metal–metal separation, the H_{ab} values presented in Table 3 represent lower limits for the electronic coupling parameter. The *effective* electron transfer distance was determined from Stark effect spectroscopy on the IVCT transitions.[19]

The *Effective* Electron-Transfer Distance: Stark Absorption Spectroscopy

Stark absorption spectra were obtained for the diastereo-isomers of [{Ru(bpy)₂}₂(μ-bpt⁻)]⁴⁺ in *n*-butyronitrile glass at 77 K and a field strength F_{ext} of 4.0 MV·cm⁻¹. The quantitative Liptay analysis[62] of the Stark response[63–65] yielded the dipole moment change ($|\Delta\mu_{12}|$), the angle between the transition moment and the dipole moment change (ξ), the difference polarisability (Δa), and the magnitude of the trace of the difference polarisability Tr(Δa). The results for the absorption $A(v)$ vs. v and Stark absorption $\Delta A(v)$ vs. v spectra for the diastereoisomers are pre-

sented in Table 4. The spectra for $(\Delta\Lambda/\Lambda\Delta)$-[{Ru(bpy)$_2$}$_2$(μ-bpt$^-$)]$^{4+}$ are shown in Figure 7, where panel (a) shows the unperturbed absorption spectrum, and panels (b) and (c) show the first- and second-derivatives of the absorption spectrum, respectively. The Stark spectrum and the best fit to the spectrum are shown in panel (d). The corresponding spectra for $(\Delta\Delta/\Lambda\Lambda)$-[{Ru(bpy)$_2$}$_2$(μ-bpt$^-$)]$^{4+}$ are shown in Figure S3 (Supporting Information).

The most notable features of the Stark signals in the range 3050–15000 cm^{-1} are the presence of strong second-derivative components for the IVCT transition [Figure 7 (i)] and the two lowest-energy components of the LMCT manifold [Figure 7 (ii)]. As shown in Table 4, the energies of the absorption bands at 77 K are blue-shifted relative to those reported in Table 2 at 238 K (–35 °C). Whereas the IVCT band retains a Gaussian-shaped appearance at both temperatures, the bandwidth is relatively narrower in *n*-butyronitrile glass. On the basis of the classical analysis,[59] the IVCT band characteristics at 77 K are consistent with the localized (Class II) classification for the mixed-valence species, consistent with the findings from the UV/Vis/NIR spectroelectrochemical studies at 238 K.

The results for the parameters obtained from the Liptay analysis of the IVCT and LMCT bands [Equations (iii) and (iv), Exp. Sect.] are reported in Table 4. The IVCT bands in the $\Delta\Lambda/\Lambda\Delta$ and $\Delta\Delta/\Lambda\Lambda$ diastereoisomers exhibit dipole moment changes of 5.92 ± 0.03 e·Å and 5.44 ± 0.04 e·Å, respectively. From Equations (4) and (5), diabatic distances (r_{ab}) of 6.26 ± 0.03 Å and 5.74 ± 0.04 Å were obtained for the $\Delta\Lambda/\Lambda\Delta$ and $\Delta\Delta/\Lambda\Lambda$ forms, respectively, using the $|\mu_{12}|$ values reported in Table 3.[58]

$$r_{ab} = [(r_{12})^2 + (|\mu_{12}|)^2]^{1/2} \qquad (4)$$

where $r_{12} = |\Delta\mu_{12}|/e$ $\qquad (5)$

Notably, the adiabatic charge-transfer distances for both diastereoisomers and the diabatic charge-transfer distance for the $\Delta\Delta/\Lambda\Lambda$ form are shorter than the geometrical metal–metal separation (r_{geo}), which is estimated as 6.185(10) Å from the crystal structure of the $(\Delta\Lambda/\Lambda\Delta)$-[{Ru(Me$_2$bpy)$_2$}$_2$(μ-bpt$^-$)]$^{3+}$ cation. The diabatic distance for $(\Delta\Lambda/\Lambda\Delta)$-[{Ru(bpy)$_2$}$_2$(μ-bpt$^-$)]$^{3+}$ is approximately identical to the geometrical separation. From Equation (6), Δq represents the actual amount of charge transferred in the IVCT process, and is necessarily less than e (unit electronic

charge). The quantity $(1 – \Delta q)/2$ can be identified with the amount of charge, which has been transferred prior to intervalence excitation. The adiabatic description reveals partial delocalization as a reduction in r_{12} (the *effective* charge-transfer distance) relative to r_{ab} (the true distance), whereas the diabatic description reveals delocalization as a reduction in the amount of charge (Δq) actually transferred. In the present case, Δq is estimated as ca. 95% for both diastereoisomeric forms.

$$er_{12} = (\Delta q)r_{ab} \qquad (6)$$

Accordingly, the H_{ab} parameters for the $\Delta\Lambda/\Lambda\Delta$ and $\Delta\Delta/\Lambda\Lambda$ forms are re-evaluated as 773 and 707 cm^{-1}, respectively, from Equation (2) using the r_{ab} values derived from the Stark analysis. These values are in close agreement to the estimates of 817 and 746 cm^{-1} (respectively) obtained from the application of Hush theory to the IVCT absorption bands, when the geometric metal–metal separation was employed rather than r_{ab}.[60] The results confirm the localized assignment for the systems.

Interestingly, the two dominant underlying transitions of the LMCT manifold in the region 12000–15000 cm^{-1} are well resolved at 77 K. As shown in Table 4, the LMCT transitions are characterized by dipole moment changes, which are significantly smaller than those for the IVCT transitions. It should be noted that the parameters obtained from spectral deconvolution of the LMCT manifold were somewhat arbitrary as the bands were assumed to be Gaussian-shaped. Accordingly, the apparent large differences in the Liptay parameters obtained for the first and second LMCT components should be interpreted cautiously.

As the uncertainties in the Stark-derived parameters reported in Table 4 reflect the errors obtained from the fitting procedure, the absolute error is likely to be considerably higher. The actual magnitudes will incorporate the uncertainties in the deconvolution and concentration, as well as the assumption of a value of 1.3 for the local field correction factor (f). The actual value of the latter depends on effects arising from the solvent, chromophore and counterion concentrations, which may also differ between the diastereoisomers. The shortcomings of the experimental and theoretical analysis of electroabsorption data have been discussed in detail previously by Boxer and co-workers.[66–69]

Table 4. Absorption and electroabsorption properties of the IVCT bands for the diastereoisomers of [{Ru(bpy)$_2$}$_2$(μ-bpt$^-$)]$^{4+}$ in *n*-butyronitrile glass at 77 K and a field strength of 4.0 MVcm^{-1}.[a]

Diastereoisomer	v_{max} [cm^{-1}]	$\Delta v_{1/2}$ [cm^{-1}]	$|\Delta\mu_{12}|$ [e·Å]	$|\Delta\mu_{12}|$ [D]	Ξ [b] [°]	Tr(Δa) [Å^3]	Δa [Å^3]
($\Delta\Lambda/\Lambda\Delta$)	5660	2980	5.92(3)	28.2(2)	0	8103(100)	6787(70)
	12546	1180	1.30(2)	6.19(2)	0	–139(20)	–516(50)
	13742	1354	2.44(1)	11.6(1)	0	632(30)	1135(50)
($\Delta\Delta/\Lambda\Lambda$)	5530	2815	5.44(4)	25.9(2)	0	3755(50)	3579(30)
	12470	1210	1.20(2)	5.72(3)	0	740(10)	761(150)
	13760	1640	2.38(3)	11.3(2)	0	606(50)	1755(200)

[a] The errors in the observed and calculated parameters (not tabulated) are ±10 cm^{-1} for v_{max} and $\Delta v_{1/2}$, ±2° for ξ, and ±10 Å^3 for Tr(Δa) and Δa. [b] The zero values for ξ indicate that the direction of charge displacement in the excited state is aligned with the transition moment.
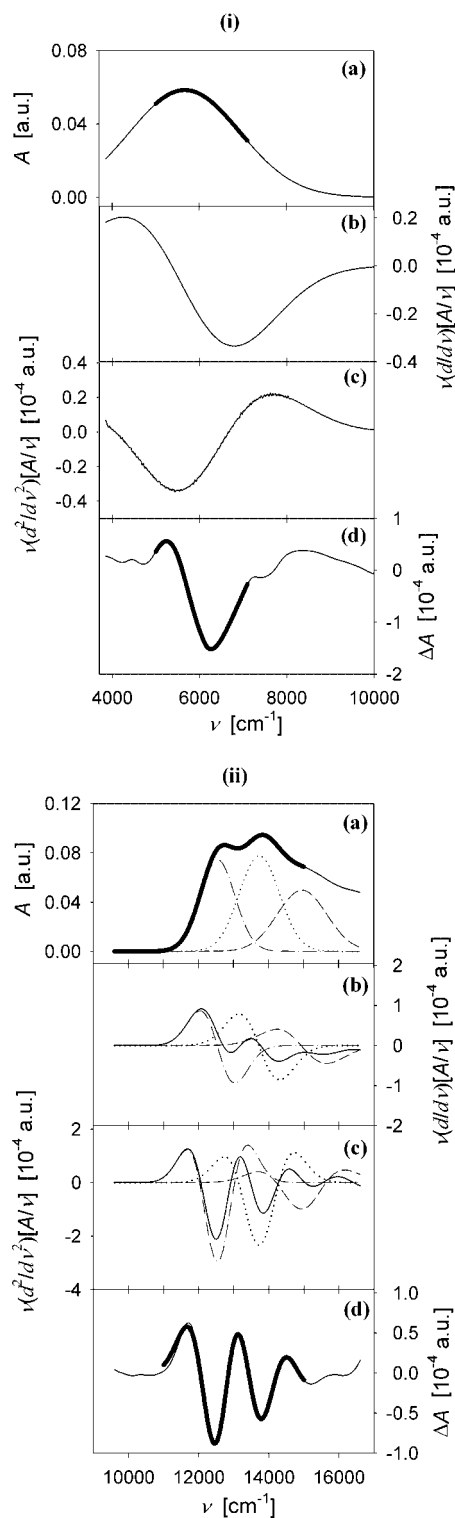
The Mechanism of Electronic Coupling

The intra-metal coupling in complexes incorporating anionic bridging ligands such as bpt⁻ is facilitated by a hole-transfer superexchange mechanism, utilising the high-lying π(bpt⁻) HOMOs of the ligand.[11,12,38,56] The situation is depicted schematically in Figure 8, where the ground state of the mixed-valence system is depicted in part (a), and the hole-transfer virtual state in (b).
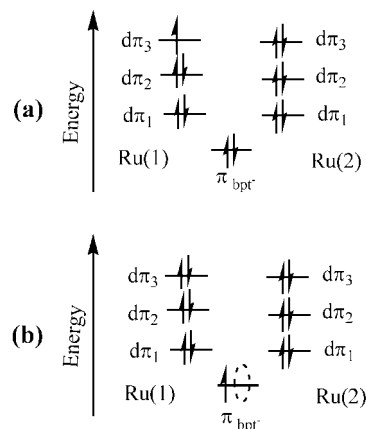

Figure 8. Schematic energy level diagram for the hole-transfer superexchange mechanism. Ground state (a) and (b) hole-transfer virtual state of the mixed-valence system [{Ru(bpy)₂}₂(μ-bpt⁻)]³⁺ showing the composition of the three Ru(dπ) orbitals and the bpt⁻ HOMO. The dotted oval represents the position of the hole on the bridging ligand.

While the σ-donor ability of N^1 site is greater than that of the N^3 site, the Ru center coordinated to N^1, denoted by Ru(1), is relatively more stabilized and undergoes oxidation prior to the Ru center coordinated to the N^3 site, denoted by Ru(2). As a consequence, the IVCT transition corresponds to the vectorial charge-transfer transition Ru(2) → Ru(1).

The similarity in the parameters of the IVCT transitions for the complexes incorporating the bpy and Me₂bpy terminal ligands demonstrates that terminal ligand variation has a minor influence on the extent of metal–metal interaction.

Stereochemical Consequences on Electron Transfer

In addition to differences between the complexes incorporating the bpy and Me₂bpy terminal ligands, measurable differences are observed in the IVCT parameters between the diastereoisomeric forms of the same complex. Whereas the origins of the stereochemical dependence of the IVCT properties is uncertain, previous studies have revealed the presence of differential solvent and anion interactions with the diastereoisomers,[16,18] in addition to differential stereochemically-induced structural distortions in the bridging ligands.[16,17] In the present case, the crystal structure of the cation in (ΔΛ/ΛΔ)-[{Ru(Me₂bpy)₂}₂(μ-bpt⁻)]³⁺ reveals a slight curvature of the bridging ligand due to steric crowd-

Figure 7. Liptay analysis of the Stark absorption spectra (*A* vs. *v*) of the (**i**) IVCT and (**ii**) LMCT transitions for (ΔΛ/ΛΔ)-[{Ru-(bpy)₂}₂(μ-bpt⁻)]⁴⁺ in *n*-butyronitrile glass at 77 K, with a field strength of 4.0 MV·cm⁻¹. (a) Unperturbed absorption spectrum with the bands obtained by Gaussian deconvolution and energy weighted first (b) and second (c) derivatives of the absorption spectrum. (d) Measured (– – –) and fitted (——) Stark signals (Δ*A* vs. *v*) at 45°. The deconvoluted components are (–·–·–·), (------) and (······).

ing between the methyl groups on the terminal ligands. However, this minor distortion is expected to be similar for the corresponding $\Delta\Delta/\Lambda\Lambda$ form, and should be negligible for both diastereoisomers of the complex incorporating the terminal bpy ligands, as described above. The stereochemical dependence of the IVCT parameters is therefore likely to arise from differential solvent and anion interactions with the two forms. Indeed, a recent report has demonstrated that differential anion interactions with the diastereoisomers of $[\{Ru(bpy)_2\}_2(\mu\text{-bpt}^-)]^{4+}$ lead to differences in the electrochemical potentials of the metal-based redox processes in the presence of the strongly ion-pairing electrolyte $[(n\text{-}C_4H_9)_4N]PF_6$ (employed in the present study) and the weakly ion-pairing electrolyte $[(n\text{-}C_4H_9)_4]\{B(C_6F_5)_4\}$.[53,70]

Conclusions

The synthesis and chromatographic separation of the diastereoisomeric forms of the complexes $[\{Ru(pp)_2\}_2(\mu\text{-bpt}^-)]^{3+}$ (pp = bpy, Me$_2$bpy) has permitted an investigation of the dependence of the IVCT properties of their mixed-valence forms on the stereochemical relationship of the metal centers. The *effective* metal–metal charge-transfer distances in the complexes incorporating the bpy terminal ligands were determined as 5.92 ± 0.03 Å for the $\Delta\Lambda/\Lambda\Delta$ form, and 5.44 ± 0.04 Å for the $\Delta\Delta/\Lambda\Lambda$ form, from Stark effect spectroscopy. These distances correspond to approximately 95 and 88%, respectively, of the geometrical metal–metal distance of 6.185(10) Å, obtained from the X-ray crystal structure of the cation in $(\Delta\Lambda/\Lambda\Delta)\text{-}[\{Ru(Me_2bpy)_2\}_2\text{-}(\mu\text{-bpt}^-)](PF_6)_3$. A classical analysis of the results from the IVCT absorption and electroabsorption spectra are consistent with a localized Class II classification for the mixed-valence systems.

Experimental Section

Materials: Potassium hexafluorophosphate (KPF$_6$; Aldrich, 98%), ammonium hexafluorophosphate (NH$_4$PF$_6$; Aldrich, 99.99%), nitrosonium hexafluorophosphate (NOPF$_6$ stored under Ar; Alfa Aesar, 96%), ethylene glycol (Ajax, 95%), sodium toluene-4-sulfonate (Aldrich, 98%), DOWEX® 1×8, 50–100 mesh (Aldrich) anion-exchange resin and laboratory reagent solvents were used as received. Tetra-*n*-butylammonium hexafluorophosphate ($[(n\text{-}C_4H_9)_4N]PF_6$; Fluka, 99+%) was dried in vacuo at 60 °C prior to use and ferrocene (Fc; BDH) was purified by sublimation prior to use. SP Sephadex C-25 (Amersham Pharmacia Biotech), and silica gel (200–400 mesh, 60 Å, Aldrich) were employed for the chromatographic separation and purification of ruthenium complexes. Acetonitrile (CH$_3$CN; Aldrich, 99.9+%) was distilled from over CaH$_2$ prior to use and *n*-butyronitrile (Aldrich, 99+%) was used as received.

General: 1D and 2D ^{1}H NMR spectra were collected with a Varian Mercury 300 MHz spectrometer. ^{1}H NMR chemical shifts for all complexes are reported relative to 99.9% [D$_3$]acetonitrile [CD$_3$CN, Cambridge Isotope Laboratories (CIL)] at $\delta = 1.93$ ppm. ^{1}H NMR assignments were performed with the assistance of COSY experiments to identify each pyridine ring system.

Electrochemistry: Electrochemical measurements were performed under argon using a Bioanalytical Systems (BAS) 100A Electrochemical Analyser. Cyclic (CV) and differential pulse (DPV) voltammograms were recorded in a standard three-electrode cell using a glassy carbon or platinum button working electrode, a platinum wire auxiliary electrode and an Ag/AgCl reference electrode (0.1 M $[(n\text{-}C_4H_9)_4N]PF_6$ in CH$_3$CN). Ferrocene was added as an internal standard on completion of each experiment; the ferrocene/ferrocenium couple (Fc$^+$/Fc^0) occurred at +550 mV vs. Ag/AgCl. Solutions contained 0.1 M $[(n\text{-}C_4H_9)_4N]PF_6$ as electrolyte. Cyclic voltammetry was performed with a sweep rate of 100 mVs^{-1}; differential pulse voltammetry was conducted with a sweep rate of 4 mVs^{-1} and a pulse amplitude, width and period of 50 mV, 60 ms and 1 s, respectively. All potentials are reported ±3 mV.

UV/Vis/NIR Spectroelectrochemistry: UV/Vis/NIR spectroelectrochemistry was performed using a CARY 5E spectrophotometer interfaced to Varian WinUV software. The absorption spectra of the electrogenerated mixed-valence species were obtained in situ by the use of a cryostatted Optically Semi-Transparent Thin-Layer Electrosynthetic (OSTLE) cell.[71] An account of the procedure employed in the spectroelectrochemical measurements has been detailed previously.[72] Solutions for the spectroelectrochemial experiments contained 0.1 M $[(n\text{-}C_4H_9)_4N]PF_6$ supporting electrolyte in CH$_3$CN and the complex (ca. $1\cdot10^{-3}$ M).

The analysis and spectral deconvolution of the data were performed as described in a previous report.[17] The IVCT spectra were scaled as $\int\varepsilon(v)/v\cdot dv$[14,73] and deconvolution of the NIR transitions was performed using the curve-fitting subroutine implemented within the GRAMS32 commercial software package.[72] On the basis of the reproducibility of the parameters obtained from the deconvolutions, the uncertainties in the energies v_{max}, intensities $(\varepsilon/v)_{max}$ and bandwidths $\Delta v_{1/2}$ were estimated as ±10 cm^{-1}, ±0.001 M^{-1} and ±10 cm^{-1}, respectively. The transition moment $|\mu_{12}|$ in e·Å is defined by Equation (ii) where the zeroth-moment, M_0, represents the area under the band of the reduced absorption spectrum.

$$M_0 = \int_{v_1}^{v_2} f(v)dv \tag{i}$$

$$|\mu_{12}| = 0.0206 \text{ Å} \times M_0^{1/2} \tag{ii}$$

Stark Absorption Spectroscopy: Detailed accounts of the instrumentation, sample preparation and analysis have been reported previously.[63,64] In a typical experiment, the un-oxidized complex (ca. 5 mg) was dissolved in *n*-butyronitrile (1 mL) and the mixed-valence species was generated by chemical oxidation with NOPF$_6$ (saturated solution in *n*-butyronitrile, 1 mL).

Stark absorption measurements were performed in a dual liquid-nitrogen immersion cryostat (Janis Research Corporation) at 77 K.[74] The electroabsorption cell consisted of two indium-tin oxide (ITO) coated quartz slides (Delta Technologies) separated by 100 µm Kapton spacers (DuPont). Electroabsorption measurements were performed at 77 K and a field strength of 4.0 MV·cm^{-1} using a CARY-14 spectrophotometer featuring OLIS control software. Dry nitrogen gas was blown over the dewar windows to prevent fogging. Electroabsorption measurements over the range 3850–12500 cm^{-1} were recorded with a photovoltaic HgCdTe detector that was thermoelectrically cooled to –40 °C (Judson Technologies), and a DE110 Silicon photodiode for measurements over the range 9090–20000 cm^{-1}.

The analysis of the data was performed according to the method of Liptay,[47] as described in detail elsewhere.[63–65] Each Stark spectrum, obtained from duplicate experiments at two angles (90° and 45°), was fitted to a linear combination of the zeroth-, first- and second-derivatives of the absorption spectrum (at 77 K) to yield values for the coefficients, A_χ, B_χ and C_χ in Equation (iii).

$$\Delta A(\nu) = \left\{ A_\chi A(\nu) + \frac{B_\chi \nu}{15hc} \frac{d[A(\nu)/\nu]}{d\nu} + \frac{C_\chi \nu}{30h^2c^2} \frac{d^2[A(\nu)/\nu]}{d\nu^2} \right\} \mathbf{F}_{int}^2 \quad \text{(iii)}$$

Here, χ is the experimental angle between $\mathbf{F}_{ext}$ and the polarization of the incident light, h is Planck's constant, and c is the speed of light in a vacuum. $\mathbf{F}_{int}$ represents the internal electric field experienced by the chromophore, and is given by $f \times \mathbf{F}_{ext}$, where f is the local-field correction factor (typically assumed to be 1.3 for organic solvents[19]). The coefficients A_χ, B_χ and C_χ provide information on changes in the transition dipole moment, and the excited state/ground-state polarisability and dipole moment differences, respectively, according to Equation (iv).

$$A_\chi = \frac{\langle \alpha_m \rangle}{3} + \frac{1}{30}(3\cos^2\chi - 1)[3\langle \beta_m \rangle - 2\langle \alpha_m \rangle]$$

$$B_\chi = \frac{5}{2}\text{Tr}(\Delta\alpha) + (3\cos^2\chi - 1)[\frac{3}{2}\hat{\mathbf{g}} \cdot \Delta\alpha \cdot \hat{\mathbf{g}} - \frac{1}{2}\text{Tr}(\Delta\alpha)]$$

$$C_\chi = |\mu_\nu|^2 [5 + (3\cos^2\xi - 1)(3\cos^2\chi - 1)] \quad \text{(iv)}$$

In these Equations, $\langle a_m \rangle$ and $\langle \beta_m \rangle$ are the scalar functions of the transition-moment polarisability and hyperpolarisability tensors, $\text{Tr}(\Delta a)$ is the trace of the polarisability change between the ground and excited electronic states, $\hat{\mathbf{g}} \cdot \Delta a \cdot \hat{\mathbf{g}}$ is the polarisability change along the transition moment ($\hat{\mathbf{g}}$ is the unit vector), $|\mu\nu|$ is the vector change in dipole moment (its sign is not determined), and ξ is the angle between the transition dipole moment and change in dipole moment vectors.[21] Measurement of Stark spectra at two or more values of χ (incident angle of polarized light in relation to the electric field) are fitted to a sum of the zeroth-, first- and second-derivatives of the absorption spectrum to yield values for the molecular parameters according to Equation (iv).

While the Liptay treatment interprets first-derivative (*i.e.* B_χ) contributions in Equations (iii) and (iv) in terms of polarisability changes, for the special case of symmetrical mixed-valence systems significant non-Liptay contributions due to field-induced changes in degenerate ground-state populations can be expected. For simplicity, we report B_χ only in terms of apparent polarisability changes.[75]

Synthetic Procedures

3,5-Bis(2-pyridyl)-1,2,4-triazole (Hbpt)[11,76] and *cis*-[Ru(pp)₂Cl₂]· 2H₂O (pp = bpy, Me₂bpy)[77] were prepared according to the literature methods.

[{Ru(bpy)₂}₂(μ-bpt⁻)](PF₆)₃: A suspension of Hbpt (21 mg, 0.094 mmol) in ethylene glycol (10 mL) was heated in a modified microwave oven (Model R-2V55; 600 W, 2450 MHz) on medium-high power[41] for 20 s to complete dissolution. *cis*-[Ru(bpy)₂Cl₂]· 2H₂O (100 mg, 0.207 mmol) was added and the mixture heated at reflux for a further 8 min during which time the solution attained a red-orange coloration. The mixture was diluted with water (ca. 50 mL) and the dinuclear product was separated from the crude mixture by a gradient elution procedure on SP Sephadex C-25 support using aqueous 0.1–0.5 M NaCl. A band of mononuclear mate-

rial eluted first (0.2 M NaCl), followed by the desired orange product (0.4 M NaCl), which was precipitated as the PF₆⁻ salt by addition of a saturated aqueous solution of KPF₆. The solid was isolated by vacuum filtration and washed with diethyl ether (3·10 mL). Yield: 93 mg (66%). The separation of the diastereoisomers was achieved by cation-exchange chromatography on SP Sephadex C-25 support (dimensions 96 cm length, 1.6 cm diameter). The complex (ca. 100 mg) was loaded onto the column in aqueous solution (as the Cl⁻ form, obtained by stirring an aqueous suspension of the complex with DOWEX® 1×8 anion exchange resin) and eluted with 0.15 M sodium toluene-4-sulfonate solution.[41] The diastereoisomers separated after passing through an effective column length of 1.5 m. The two bands were collected, and the products were precipitated by the addition of a saturated aqueous KPF₆ solution. The solids were isolated by vacuum filtration and washed with diethyl ether (3×10 mL).

Rigorous purification methods were employed prior to characterization because of the potentially strong associations between the complex cations and the anions present in the eluents employed for the chromatographic separations.[41,46] Each product was dissolved in a minimum volume of acetone and loaded onto a short column of silica gel (dimensions: 2 cm diameter, 4 cm length), washed with acetone, water and acetone and then eluted with acetone containing 5% NH₄PF₆. Addition of water and removal of the acetone under reduced pressure afforded a product of suitable purity for the physical measurements. Band 1 and band 2 exhibited different NMR spectra, with the former identified as the ΔΛ/ΛΔ and the latter as the ΔΔ/ΛΛ diastereoisomers. ¹H NMR (CD₃CN): δ (**Band 1; ΔΛ/ΛΔ**) = 6.40 (dd, J = 8, 1.5 Hz, 1 H, H3 bpt⁻), 6.82 (dd, J = 8, 1.5 Hz, 1 H, H3′ bpt⁻), 6.92 (t, J = 8, 5 Hz, 1 H, H5 bpt⁻), 7.00 (dd, J = 8, 8 Hz, 1 H, H4 bpt⁻), 7.04 (dd, J = 8, 8 Hz, 1 H, H4′ bpt⁻), 7.12 (t, J = 8, 5 Hz, 1 H, H5 bpy), 7.23 (t, J = 8, 5 Hz, 3 H, H5 bpy), 7.27 (t, J = 8, 5 Hz, 1 H, H5 bpy), 7.33 (t, J = 8, 5 Hz, 2 H, H5 bpy), 7.53 (dd, J = 5, 1.5 Hz, 1 H, H6 bpt⁻), 7.56 (t, J = 8, 5 Hz, 1 H, H5 bpy), 7.63 (dd, J = 5, 1.5 Hz, 1 H, H6 bpy), 7.66 (dd, J = 5, 1.5 Hz, 1 H, H6 bpy), 7.74 (dd, J = 5, 1.5 Hz, 1 H, H6 bpy), 7.76 (dd, J = 5, 1.5 Hz, 1 H, H6 bpy), 7.79 (t, J = 8, 5 Hz, 1 H, H5′ bpt⁻), 7.81 (dd, J = 5, 1.5 Hz, 1 H, H6 bpy), 7.85 (dd, J = 8, 8 Hz, 2 H, H4 bpy), 7.88 (dd, J = 5, 1.5 Hz, 1 H, H6 bpy), 7.89 (dd, J = 8, 8 Hz, 3 H, H4 bpy), 7.94 (dd, J = 8, 8 Hz, 2 H, H4 bpy), 7.98 (dd, J = 5, 1.5 Hz, 2 H, H6 bpy), 8.01 (dd, J = 8, 8 Hz, 1 H, H4 bpy), 8.33 (dd, J = 8, 1.5 Hz, 1 H, H3 bpy), 8.36 (dd, J = 8, 1.5 Hz, 1 H, H3 bpy), 8.43 (dd, J = 8, 1.5 Hz, 1 H, H3 bpy), 8.44 (dd, J = 5, 1.5 Hz, 1 H, H6′ bpt⁻), 8.45 (dd, J = 8, 1.5 Hz, 1 H, H3 bpy), 8.48 (dd, J = 8, 1.5 Hz, 2 H, H3 bpy), 8.52 (dd, J = 8, 1.5 Hz, 2 H, H3 bpy); δ (**Band 2; ΔΔ/ΛΛ**) = 6.54 (dd, J = 8, 1.5 Hz, 1 H, H3 bpt⁻), 6.98 (dd, J = 8, 1.5 Hz, 1 H, H3′ bpt⁻), 6.86 (t, J = 8, 5 Hz, 1 H, H5 bpt⁻), 7.06 (dd, J = 8, 8 Hz, 1 H, H4 bpt⁻), 7.42 (dd, J = 8, 8 Hz, 1 H, H4′ bpt⁻), 7.44 (dd, J = 5, 1.5 Hz, 1 H, H6 bpt⁻), 7.89 (t, J = 8, 5 Hz, 1 H, H5′ bpt⁻), 8.38 (dd, J = 5, 1.5 Hz, 1 H, H6′ bpt⁻), 7.31 (dd, J = 5, 1.5 Hz, 1 H, H6 bpy), 7.38 (dd, J = 5, 1.5 Hz, 1 H, H6 bpy), 6.90-7.20 (5 H, H5 bpy), 7.89 (dd, J = 8, 8 Hz, 1 H, H4 bpy), 7.92 (dd, J = 8, 8 Hz, 1 H, H4 bpy), 7.70-8.00 (5 H, H4 bpy), 7.70-8.00 (5 H, H6 bpy), 7.98 (dd, J = 5, 1.5 Hz, 1 H, H6 bpy), 8.13 (dd, J = 5, 1.5 Hz, 1 H, H6 bpy), 8.54 (dd, J = 8, 1.5 Hz, 1 H, H3 bpy), 8.60 (dd, J = 8, 1.5 Hz, 1 H, H3 bpy), 8.30-8.60 (J = 8, 1.5 Hz, 5 H, H3 bpy) ppm.

[{Ru(Me₂bpy)₂}₂(μ-bpt⁻)](PF₆)₃: This compound was prepared from Hbpt (19 mg, 0.084 mmol) and [Ru(Me₂bpy)₂Cl₂]·2H₂O (100 mg, 0.18 mmol) by a procedure analogous to that detailed above for [{Ru(bpy)₂}₂(μ-bpt⁻)](PF₆)₃. Yield: 107 mg (67%). The separation of the diastereoisomers was achieved by cation-exchange chromatography on SP Sephadex C-25 support using 0.15 M so-

D. M. D'Alessandro, P. H. Dinolfo, J. T. Hupp, P. C. Junk, F. R. Keene

dium toluene-4-sulfonate solution as the eluent. Band 1 and band 2 exhibited different NMR spectra, with the former identified as the $\Delta\Lambda/\Lambda\Delta$ and the latter as the $\Delta\Delta/\Lambda\Lambda$ diastereoisomers. ¹H NMR (CD₃CN): δ (**Band 1; $\Delta\Lambda/\Lambda\Delta$**) = 2.45 (s, 6 H, CH₃), 2.48 (s, 6 H, CH₃), 2.51 (s, 6 H, CH₃), 2.57 (s, 6 H, CH₃), 6.38 (dd, J = 8, 1.5 Hz, 1 H, H3 bpt⁻), 6.81 (dd, J = 8, 1.5 Hz, 1 H, H3′ bpt⁻), 6.90 (t, J = 8, 5 Hz, 1 H, H5 bpt⁻), 7.02 (dd, J = 8, 8 Hz, 1 H, H4 bpt⁻), 7.06 (dd, J = 8, 8 Hz, 1 H, H4′ bpt⁻), 7.05 (d, J = 6 Hz, 1 H, H5 Me₂bpy), 7.23 (d, J = 6 Hz, 3 H, H5 Me₂bpy), 7.23 (d, J = 6 Hz, 1 H, H5 Me₂bpy), 7.29 (d, J = 6 Hz, 2 H, H5 Me₂bpy), 7.51 (dd, J = 5, 1.5 Hz, 1 H, H6 bpt⁻), 7.52 (d, J = 6 Hz, 1 H, H5 Me₂bpy), 7.59 (d, J = 6 Hz, 1 H, H6 Me₂bpy), 7.63 (d, J = 6 Hz, 1 H, H6 Me₂bpy), 7.70 (d, J = 6 Hz, 1 H, H6 Me₂bpy), 7.71 (d, J = 6 Hz, 1 H, H6 Me₂bpy), 7.76 (t, J = 8, 5 Hz, 1 H, H5′ bpt⁻), 7.77 (d, J = 6 Hz, 1 H, H6 Me₂bpy), 7.83 (d, J = 6 Hz, 1 H, H6 Me₂bpy), 7.95 (d, J = 6 Hz, 2 H, H6 Me₂bpy), 8.27 (s, 1 H, H3 Me₂bpy), 8.33 (s, 1 H, H3 Me₂bpy), 8.40 (s, 1 H, H3 Me₂bpy), 8.41 (dd, J = 5, 1.5 Hz, 1 H, H6′ bpt⁻), 8.37 (s, 1 H, H3 Me₂bpy), 8.46 (s, 2 H, H3 Me₂bpy), 8.49 (s, 2 H, H3 Me₂bpy); δ (**Band 2; $\Delta\Delta/\Lambda\Lambda$**) = 2.47 (s, 12 H, CH₃), 2.50 (s, 6 H, CH₃), 2.53 (s, 6 H, CH₃), 6.51 (dd, J = 8, 1.5 Hz, 1 H, H3 bpt⁻), 6.95 (dd, J = 8, 1.5 Hz, 1 H, H3′ bpt⁻), 6.81 (t, J = 8, 5 Hz, 1 H, H5 bpt⁻), 7.39 (dd, J = 8, 8 Hz,1 H, H4′ bpt⁻), 7.42 (dd, J = 5, 1.5 Hz, 1 H, H6 bpt⁻), 7.85 (t, J = 8, 5 Hz, 1 H, H5′ bpt⁻), 8.32 (dd, J = 5, 1.5 Hz, 1 H, H6′ bpt⁻), 7.26 (d, J = 6 Hz, 1 H, H6 Me₂bpy), 7.35 (d, J = 6 Hz, 1 H, H6 Me₂bpy), 6.80-7.15 (5 H, H5 Me₂bpy), 7.63-7.95 (5 H, H6 Me₂bpy), 7.94 (d, J = 6 Hz, 1 H, H6 Me₂bpy), 8.07 (d, J = 6 Hz, 1 H, H6 Me₂bpy), 8.51 (s, 1 H, H3 Me₂bpy), 8.57 (s, 1 H, H3 Me₂bpy), 8.22-8.55 (5 H, H3 Me₂bpy) ppm.

X-ray Crystallography: Single crystals of $(\Delta\Lambda/\Lambda\Delta)$-[{Ru-(Me₂bpy)₂}₂($\mu$-bpt⁻)](PF₆)₃ were obtained by dissolution of ca. 1 mmol of the complex in acetone/water (1:1, 2 mL). Slow evaporation of the solution at room temperature yielded dark red rod-shaped crystals suitable for X-ray determination. The collection and refinement of X-ray data was performed in the Advanced Analytical Centre at James Cook University. Hemispheres of data were collected (capillary sealed specimens) at room temperature with a Bruker SMART CCD diffractometer using the omega scan mode. A summary of the data collection and refinement details is provided in Table S1 of the Supporting Information. Data sets were corrected for absorption using the program SADABS.[78] The solution and refinement for all structures was carried out using SHELXL-97[79] utilising the graphical interface X-Seed.[80] Crystallographic data (excluding structure factors) for the structure reported in this paper have been deposited with the Cambridge Crystallographic Data Centre as supplementary publication no. CCDC-286553 contains the supplementary crystallographic data for this paper. These data can be obtained free of charge from The Cambridge Crystallographic Data Centre via www.ccdc.cam.ac.uk/data_request/cif.

Supporting Information (for details see the footnote on the first page of this article): Proton numbering schemes for NMR characterization (Figure S1), spectroelectrochemical progression for [Ru(bpy)₂(bpt⁻)]⁺/²⁺ (Figure S2) and Stark absorption spectra for $(\Delta\Delta/\Lambda\Lambda)$-[{Ru(bpy)₂}₂($\mu$-bpt⁻)]³⁺ (Figure S3).

Acknowledgments

[1] V. Balzani, A. Juris, M. Venturi, S. Campagna, S. Serroni, *Chem. Rev.* **1996**, *96*, 759–833.
[2] K. Kalyanasundaram, M. K. Nazeeruddin, *Inorg. Chim. Acta* **1994**, *226*, 213–230.
[3] M. D. Ward, *Chem. Soc. Rev.* **1995**, *24*, 121–134.
[4] D. E. Richardson, H. Taube, *J. Am. Chem. Soc.* **1983**, *105*, 40–51.
[5] D. E. Richardson, H. Taube, *Coord. Chem. Rev.* **1984**, *60*, 107–129.
[6] G. Giuffrida, S. Campagna, *Coord. Chem. Rev.* **1994**, *135*, 517–531.
[7] M. D. Newton, *Chem. Rev.* **1991**, *91*, 767–792.
[8] C. G. Garcia, J. F. de Lima, N. Y. M. Iha, *Coord. Chem. Rev.* **2000**, *196*, 219–247.
[9] F. Barigelletti, L. De Cola, V. Balzani, R. Hage, J. G. Haasnoot, J. Reedijk, J. G. Vos, *Inorg. Chem.* **1991**, *30*, 641–645.
[10] H. M. McConnell, *J. Chem. Phys.* **1961**, *35*, 508–515.
[11] R. Hage, A. H. J. Dijkhuis, J. G. Haasnoot, R. Prins, J. Reedijk, B. E. Buchanan, J. G. Vos, *Inorg. Chem.* **1988**, *27*, 2185–2189.
[12] R. Hage, J. G. Haasnoot, H. A. Nieuwenhuis, J. Reedijk, D. J. A. De Ridder, J. G. Vos, *J. Am. Chem. Soc.* **1990**, *112*, 9245–9251.
[13] B. E. Buchanan, R. Wang, J. G. Vos, R. Hage, J. P. Haasnoot, J. Reedijk, *Inorg. Chem.* **1990**, *29*, 3263–3265.
[14] N. S. Hush, *Prog. Inorg. Chem.* **1967**, *8*, 391–444.
[15] N. S. Hush, *Electrochim. Acta* **1968**, *13*, 1005–1023.
[16] D. M. D'Alessandro, L. S. Kelso, F. R. Keene, *Inorg. Chem.* **2001**, *40*, 6841–6844.
[17] D. M. D'Alessandro, P. C. Junk, F. R. Keene, *Supramol. Chem.* **2005**, in press.
[18] D. M. D'Alessandro, F. R. Keene, *Chem. Phys.* **2005**, in press.
[19] G. U. Bublitz, S. G. Boxer, *Annu. Rev. Phys. Chem.* **1997**, *48*, 213–242.
[20] B. S. Brunschwig, C. Creutz, N. Sutin, *Coord. Chem. Rev.* **1998**, *177*, 61–79.
[21] K. A. Walters, *Comprehensive Coord. Chem. II* **2003**, *2*, 303–313.
[22] A. Ferretti, *Coord. Chem. Rev.* **2003**, *238–239*, 127–141.
[23] F. W. Vance, R. D. Williams, J. T. Hupp, *Int. Rev. Phys. Chem.* **1998**, *17*, 307–329.
[24] W. R. Browne, C. M. O'Connor, C. Villani, J. G. Vos, *Inorg. Chem.* **2001**, *40*, 5461–5464.
[25] R. Hage, *Coord. Chem. Rev.* **1991**, *111*, 161–166.
[26] B. E. Buchanan, J. G. Vos, M. Kaneko, W. J. M. van der Putten, J. M. Kelly, R. Hage, R. A. G. de Graaff, J. G. Haasnoot, J. Reedijk, *J. Chem. Soc., Dalton Trans.* **1990**, 2425–2431.
[27] J. H. van Diemen, R. Hage, J. G. Haasnoot, H. E. B. Lempers, J. Reedijk, J. G. Vos, L. De Cola, F. Barigelletti, V. Balzani, *Inorg. Chem.* **1992**, *31*, 3518–3522.
[28] R. Hage, J. G. Haasnot, D. J. Stufkens, T. L. Snoeck, J. G. Vos, J. Reedijk, *Inorg. Chem.* **1989**, *28*, 1413–1414.
[29] L. De Cola, F. Barigelletti, V. Balzani, R. Hage, J. G. Haasnoot, J. Reedijk, J. G. Vos, *Chem. Phys. Lett.* **1991**, *178*, 491–496.
[30] W. R. Browne, C. M. O'Connor, H. P. Hughes, R. Hage, O. Walter, M. Doering, J. F. Gallagher, J. G. Vos, *J. Chem. Soc., Dalton Trans.* **2002**, 4048–4054.
[31] G. Giuffrida, G. Calogero, G. Guglielmo, V. Ricevuto, S. Campagna, *Inorg. Chim. Acta* **1996**, *251*, 255–264.
[32] G. Giuffrida, G. Calogero, V. Ricevuto, S. Campagna, *Inorg. Chem.* **1995**, *34*, 1957–1960.
[33] H. P. Hughes, D. Martin, S. Bell, J. J. McGarvey, J. G. Vos, *Inorg. Chem.* **1993**, *32*, 4402–4408.

[34] G. Giuffrida, G. Calogero, G. Guglielmo, V. Ricevuto, M. Ciano, S. Campagna, *Inorg. Chem.* **1993**, *32*, 1179–1183.

[35] G. Giuffrida, V. Ricevuto, G. Guglielmo, S. Campagna, M. Ciano, *Inorg. Chim. Acta* **1992**, *194*, 23–29.

[36] R. Sahai, D. P. Rillema, R. Shaver, S. Van Wellendael, D. C. Jackman, M. Boldaji, *Inorg. Chem.* **1989**, *28*, 1022–1028.

[37] F. Barigelletti, L. De Cola, V. Balzani, R. Hage, J. G. Haasnoot, J. Reedijk, J. G. Vos, *Inorg. Chem.* **1989**, *28*, 4344–4350.

[38] C. Di Pietro, S. Serroni, S. Campagna, M. T. Gandolfi, R. Ballardini, S. Fanni, W. R. Browne, J. G. Vos, *Inorg. Chem.* **2002**, *41*, 2871–2878.

[39] A. C. Lees, C. J. Kleverlaan, C. A. Bignozzi, J. G. Vos, *Inorg. Chem.* **2001**, *40*, 5343–5349.

[40] K. F. Mongey, J. G. Vos, B. D. MacCraith, C. M. McDonagh, *Coord. Chem. Rev.* **1999**, *185–186*, 417–429.

[41] N. C. Fletcher, P. C. Junk, D. A. Reitsma, F. R. Keene, *J. Chem. Soc., Dalton Trans.* **1998**, 133–138.

[42] L. S. Kelso, PhD Thesis, James Cook University, Townsville, Australia, **2000**.

[43] B. D. Yeomans, L. S. Kelso, P. A. Tregloan, F. R. Keene, *Eur. J. Inorg. Chem.* **2001**, 239–246.

[44] T. J. Rutherford, O. Van Gijte, A. Kirsch-De Mesmaeker, F. R. Keene, *Inorg. Chem.* **1997**, *36*, 4465–4474.

[45] P. A. Adcock, F. R. Keene, R. S. Smythe, M. R. Snow, *Inorg. Chem.* **1984**, *23*, 2336–2343.

[46] N. C. Fletcher, F. R. Keene, *J. Chem. Soc., Dalton Trans.* **1999**, 683–689.

[47] X. Hua, PhD Thesis, University of Fribourg, Fribourg, Switzerland, **1993**.

[48] E. C. Constable, J. Lewis, *Inorg. Chim. Acta* **1983**, *70*, 251–253.

[49] V. Balzani, D. A. Bardwell, F. Barigelletti, F. L. Cleary, M. Guardigli, J. C. Jeffery, T. Sovrani, M. D. Ward, *J. Chem. Soc., Dalton Trans. J. Chem. Soc., Dalton Trans* **1995**, 3601–3608.

[50] R. Hage, J. P. Turkenburg, R. A. G. de Graaff, J. G. Haasnoot, J. Reedijk, *Acta Crystallogr., Sect. A Acta Crystallogr.* **1989**, *45*, 381–383.

[51] D. P. Rillema, D. G. Taghdiri, D. S. Jones, C. D. Keller, L. A. Worl, T. J. Meyer, H. A. Levy, *Inorg. Chem.* **1987**, *26*, 578–585.

[52] D. P. Rillema, D. S. Jones, H. A. Levy, *J. Chem. Soc., Chem. Commun.* **1979**, 849–851.

[53] D. M. D'Alessandro, F. R. Keene, *Dalton Trans.* **2004**, 3950–3954.

[54] A. Juris, S. Barigelletti, S. Campagna, V. Balzani, P. Belser, A. von Zelewsky, *Coord. Chem. Rev.* **1988**, *84*, 85–277.

[55] K. A. Goldsby, T. J. Meyer, *Inorg. Chem.* **1984**, *23*, 3002–3010.

[56] R. Hage, J. G. Haasnoot, J. Reedijk, R. Wang, J. G. Vos, *Inorg. Chem.* **1991**, *30*, 3263–3269–3275.

[57] C. Creutz, M. D. Newton, N. Sutin, *J. Photochem. Photobiol., A* **1994**, *82*, 47–59.

[58] R. J. Cave, M. D. Newton, *Chem. Phys. Lett.* **1996**, *249*, 15–19.

[59] K. D. Demadis, C. M. Hartshorn, T. J. Meyer, *Chem. Rev.* **2001**, *101*, 2655–2685.

[60] N. S. Hush, *Coord. Chem. Rev.* **1985**, *64*, 135–157.

[61] M. B. Robin, P. Day, *Adv. Inorg. Chem. Radiochem.* **1967**, *10*, 247–403.

[62] W. Liptay, *Angew. Chem. Int. Ed. Engl.* **1969**, *8*, 177–188.

[63] L. Karki, J. T. Hupp, *Inorg. Chem.* **1997**, *36*, 3318–3321.

[64] P. H. Dinolfo, J. T. Hupp, *J. Am. Chem. Soc.* **2004**, *126*, 16814–16819.

[65] Y. G. K. Shin, B. S. Brunschwig, C. Creutz, N. Sutin, *J. Phys. Chem.* **1996**, *100*, 8157–8169.

[66] D. H. Oh, M. Sano, S. G. Boxer, *J. Am. Chem. Soc.* **1991**, *113*, 6880–6890.

[67] G. U. Bublitz, S. G. Boxer, *J. Am. Chem. Soc.* **1998**, *120*, 3988–3992.

[68] Y. G. K. Shin, B. S. Brunschwig, C. Creutz, N. Sutin, *J. Phys. Chem.* **1996**, *100*, 8157–8169.

[69] Y. G. K. Shin, B. S. Brunschwig, C. Creutz, N. Sutin, *J. Am. Chem. Soc.* **1995**, *117*, 8668–8669.

[70] R. LeSuer, W. E. Geiger, *Angew. Chem. Int. Ed.* **2000**, *39*, 248–250.

[71] C. M. Duff, G. A. Heath, *Inorg. Chem.* **1991**, *30*, 2528–2535.

[72] D. M. D'Alessandro, F. R. Keene, *Chem. Eur. J.* **2005**, *11*, 3679–3688.

[73] J. R. Reimers, N. S. Hush, *Inorg. Chem.* **1990**, *29*, 3686–3697.

[74] S. S. Andrews, S. G. Boxer, *Rev. Sci. Instrum.* **2000**, *71*, 3567–3569.

[75] T. P. Treynor, S. G. Boxer, *J. Phys. Chem. A* **2004**, *108*, 1764–1778.

[76] J. F. Geldard, F. Lions, *J. Org. Chem.* **1965**, *30*, 318–319.

[77] T. Togano, N. Nagao, M. Tsuchida, H. Kumakura, K. Hisamatsu, F. S. Howell, M. Mukaida, *Inorg. Chim. Acta* **1992**, *195*, 221–225.

[78] R. H. Blessing, *Acta Crystallogr., Sect. A* **1995**, *51*, 33–38.

[79] G. M. Sheldrick, SHELXL-97, University of Göttingen, Göttingen, Germany, **1997**.

[80] L. J. Barbour, *J. Supramol. Chem.* **2001**, *1*, 189–191.